RAA 2018 Vol. **18** No. **5**, 57(12pp) doi: 10.1088/1674–4527/18/5/57

http://www.raa-journal.org *http://iopscience.iop.org/raa*

***R**esearch in*
***A**stronomy and*
***A**strophysics*

A low-latency pipeline for GRB light curve and spectrum using *Fermi*/GBM near real-time data

Yi Zhao[1,2], Bin-Bin Zhang[3,4], Shao-Lin Xiong[2], Xi Long[2,5], Qiang Zhang[2], Li-Ming Song[2], Jian-Chao Sun[2], Yuan-Hao Wang[2,5], Han-Cheng Li[2,5], Qing-Cui Bu[2], Min-Zi Feng[2,5], Zheng-Heng Li[2,5], Xing Wen[2,5], Bo-Bing Wu[2], Lai-Yu Zhang[2], Yong-Jie Zhang[2], Shuang-Nan Zhang[2] and Jian-Xiong Shao[1]

[1] School of Nuclear Science and Technology, Lanzhou University, Lanzhou 730000, China; *yizhao@ihep.ac.cn*
[2] Key Laboratory of Particle Astrophysics, Institute of High Energy Physics, Chinese Academy of Sciences, Beijing 100049, China; *xiongsl@ihep.ac.cn*
[3] School of Astronomy and Space Science, Nanjing University, Nanjing 210093, China
[4] Instituto de Astrofísica de Andalucía (IAA-CSIC), P.O. Box 03004, E-18080 Granada, Spain
[5] University of Chinese Academy of Sciences, Beijing 100049, China

Received 2017 December 14; accepted 2018 February 11

Abstract Rapid response and short time latency are very important for Time Domain Astronomy, such as the observations of Gamma-ray Bursts (GRBs) and electromagnetic (EM) counterparts of gravitational waves (GWs). Based on near real-time *Fermi*/GBM data, we developed a low-latency pipeline to automatically calculate the temporal and spectral properties of GRBs. With this pipeline, some important parameters can be obtained, such as T_{90} and fluence, within $\sim$ 20 min after the GRB trigger. For $\sim 90\%$ of GRBs, T_{90} and fluence are consistent with the GBM catalog results within 2σ errors. This pipeline has been used by the Gamma-ray Bursts Polarimeter (POLAR) and the *Insight* Hard X-ray Modulation Telescope (*Insight*-HXMT) to follow up the bursts of interest. For GRB 170817A, the first EM counterpart of GW events detected by *Fermi*/GBM and INTEGRAL/SPI-ACS, the pipeline gave T_{90} and spectral information 21 min after the GBM trigger, providing important information for POLAR and *Insight*-HXMT observations.

Key words: gamma-ray bursts: general — polarization — radiation mechanisms: non-thermal

1 INTRODUCTION

Gamma-ray Bursts (GRBs) are the catastrophic processes happening during either violent stellar explosions or the coalescence of binary compact stars in the Universe. Since the discovery of GRBs by the *Vela* satellites was published in 1973 (Klebesadel et al. 1973), GRBs have become a hot topic for astrophysical researches. Thereafter, many dedicated gamma-ray space telescopes, such as *CGRO*, *BeppoSAX*, *HETE-2*, *Swift* and *Fermi*, were launched to explore the properties of GRBs (Boella et al. 1997; Gehrels et al. 2004; Lin 2009; Meegan et al. 2009). The physics of GRBs, however, is still an open question (Zhang 2011; Kumar & Zhang 2015). Among them, the prompt emission mechanism of GRBs is highly uncertain. Apart from the light curve and spectral analysis, the polarization of γ-ray photons is of great importance for constraining prompt emission mechanism models. However, a precise polarization measurement is still lacking. The Gamma-ray Burst Polarimeter (POLAR), launched on-board the Chinese Space Laboratory "Tiangong-2" (TG2) on 2016 September 15, is a space-borne Compton polarimeter aiming to measure the polarization of GRB prompt emission in the 50–500 keV energy range with high accuracy (Produit et al. 2005, 2018; Suarez-Garcia et al. 2010; Orsi et al. 2011; Kole et al. 2017).

Since POLAR is the best GRB polarimeter ever flown, the most interesting GRBs for POLAR are those with high polarization measurement accuracy, i.e. low Minimum Detectable Polarization (MDP) (Lazzati 2006; Toma et al. 2009; Xiong et al. 2009). For a given GRB, MDP is determined by the location, T_{90}[1] and fluence of the GRB. However, due to limitations related to telemetry received from POLAR, no real-time data are available and the delay would be typically $\sim$ 10 hours. In order to enhance the production of science results from POLAR, a dedicated real-time alert system has been set up to monitor GRBs reported by other telescopes (e.g. *Swift* and *Fermi*/GBM) to predict whether they are visible by POLAR based on the orbit of TG2 and evaluate the MDP of those GRBs. Finally, we publicize interesting GRBs to the GRB community to encourage follow-up observations.

In order to facilitate follow-up observations, it is important to estimate the MDP with low latency. Thus, we need to derive information about the GRB location, duration and fluence at the earliest time possible after the GRB trigger. Moreover, the GRB properties mentioned above and other properties like whether a GRB is short or long, and what the spectral hardness is, are also helpful for detecting the electromagnetic (EM) counterparts of gravitational waves (GWs) (Berger 2014). Therefore, a low-latency calculation of T_{90} and fluence for GRBs is highly required.

So far, the Gamma-ray Burst Monitor (GBM) onboard the *Fermi* Gamma-ray Space Telescope is one of the most sensitive instruments for GRB detection. In the past $\sim$ 9 yr, *Fermi*/GBM has detected $\sim$ 2200 GRBs, which means $\sim$ 240 GRBs per year (Paciesas et al. 2012; von Kienlin et al. 2014; Narayana Bhat et al. 2016). In addition, *Fermi*/GBM sends a series of Gamma-ray Coordinates Network (GCN) Notices[2] (including FLT, GND and FINAL Notices) within several minutes and releases the near real-time data within $\sim$ 15 min after the GBM trigger. Although these GCN Notices can report the trigger time, the GRB location, a link to the near real-time data with counts rate (i.e. light curve) in eight energy channels, etc., no direct information about T_{90} and spectral parameters are provided.

To satisfy the requirement for POLAR, we developed a low-latency pipeline, based on the near real-time data of *Fermi*/GBM, to automatically calculate the temporal and spectral properties of GRBs, including T_{90} and fluence.

This paper is structured as follows. In Section 2, the pipeline including the data selection and reduction is briefly described. Then the performance is validated by comparing the T_{90} and spectral results analyzed by the pipeline with those of the GBM GRB catalog for 700 GRBs in Section 3. Finally, in Section 4, we summarize our results and provide a brief discussion. Unless otherwise stated, all errors adopted in this paper are given at the 1σ confidence level.

2 DESCRIPTION OF THE PIPELINE

2.1 Data Selection

The original GBM observational data are available online on the GBM data server[3]. Three types of information are required by the pipeline: science data, GRB location and GBM Detector Response Matrices (DRMs). For each burst, GBM provides three types of science data: CTIME, CSPEC and Time-Tagged Events (TTE) data. The CTIME data have fine time resolution but coarse spectral resolution. In contrast, the CSPEC data have coarse time resolution but fine spectral resolution. The TTE data consist of individual photon events with fine time resolution (2 microseconds) and fine spectral resolution (128 energy channels). In practice, GBM usually uses the CTIME or TTE data for T_{90} calculation and uses the CSPEC or TTE data for spectral analysis (Meegan et al. 2009).

Once GBM is triggered by a burst, the TRIGDAT data will be immediately downlinked through the Tracking and Data Relay Satellite System (TDRSS) in near-real time. Then it will be quickly available on the GBM data server in $\sim$ 15 min after the trigger. The TRIGDAT data include the counts rate of all 14 GBM detectors with coarse spectral resolution of eight energy channels, spanning from $T_0 - 150$ s to $T_0 + 450$ s. For the TRIGDAT data, the bin size of the counts rate is not constant. It is typically 1.024 s, and sometimes it is 0.064 s or 0.256 s for only 1–2 bins in the time region from T_0 to $T_0 + 60$ s, while for other regions it is 8.192 s (Meegan et al. 2009). Although the TRIGDAT data are not as precise as the CTIME, CSPEC and TTE data, they can be available within about 15 min after the GRB trigger, which is much faster than other types of data, as shown

[1] T_{90} is defined as the time during which cumulative counts increase from 5% to 95% above background (Kouveliotou et al. 1993).

[2] *https://gcn.gsfc.nasa.gov/fermi_grbs.html*

[3] *https://heasarc.gsfc.nasa.gov/FTP/fermi/data/gbm/bursts/*

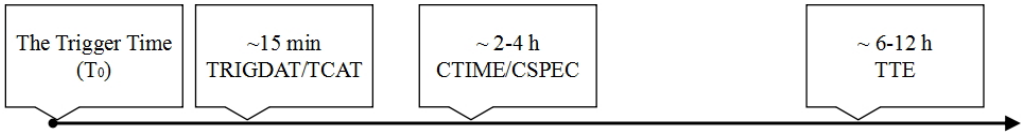

Fig. 1 Timeline of the *Fermi*/GBM data products. Our pipeline employs the TRIGDAT data as the science data and the TCAT data as the location files for the sake of timeliness.

in Figure 1. Therefore, the TRIGDAT data are chosen as the science data input of the pipeline.

GBM disseminates the GRB location information (including flight, ground and final locations) via the GCN Notice. The final location information is recorded in the TCAT data. The TCAT and TRIGDAT data usually appear on the data server at the same time. Therefore, our pipeline employs the TCAT data as location files.

The DRMs are mandatory for spectral analysis. However, the GBM-released DRM files are not available before the CTIME and CSPEC data arrive. As part of the science analysis tool provided by the GBM, the response matrix generator[4] is designated to produce the DRMs according to the trigger time and the attitude information of the spacecraft. Thus the response matrix generator is utilized by our pipeline to generate the DRMs.

2.2 Data Reduction

As shown in Figure 2, our low-latency light curve and spectral analysis pipeline mainly consist of four modules: A, B, C and D. The function of each module is described below. Detailed analysis methods are presented in the following subsections.

Module A: monitor the GCN Notice. The pipeline monitors the GCN Notices released by GBM for newly detected GRBs in real time. Once a new GBM GCN Notice arrives, the corresponding TRIGDAT and TCAT data will be automatically downloaded.

Module B: select the good detectors. The incident angles of 12 Sodium Iodide (NaI) and two Bismuth Germinate (BGO) detectors are computed according to the GRB location and the spacecraft attitude recorded in the TCAT data. Then the two NaI detectors with the minimum incident angles which are less than 60 deg and the BGO detector with the optimum incident angle (the so-called 'good detectors') are selected for the T_{90} and spectral analysis in the pipeline. Meanwhile, the DRMs can be calculated by the response matrix generator.

[4] *https://fermi.gsfc.nasa.gov/ssc/data/analysis/rmfit/gbmrsp-2.0.10.tar.bz2*

Module C: calculate T_{90}. We note that time duplicate data exist in the TRIGDAT files, which are removed by the pipeline before they are used. Once the light curve is generated, the background and burst intervals will be automatically selected through the iteration method (see Sect. 2.3). Fitting and subtracting the background will be followed, and then T_{90} will be calculated. Our pipeline also provides an option for users to choose the background and source intervals manually.

Module D: spectral analysis. The pipeline automatically analyzes the total spectra and background spectra according to the obtained T_{90}. Using the spectra and the DRM files, this pipeline will automatically fit the observational data and calculate the fluence. Complementary to the automatic fitting, manual selection of the fitting models is also provided.

Generally, near real-time data from the GMB (TRIGDAT, TCAT) can be available within $\sim$ 15 min. For most GRBs, T_{90} will be automatically calculated within 30 s and the spectral analysis results can be obtained within $\sim$ 5 min. Therefore, our pipeline can produce results within $\sim$ 20 min after trigger.

The pipeline will transfer the obtained results of T_{90} and spectral parameters to the internal web server of POLAR. These results can also be obtained by the POLAR Burst Advocates (BA) through manually selecting the background intervals, the burst intervals and the fitting models, as shown in Figure 2. In this case, another several minutes are needed considering the BA response.

2.3 T_{90} Calculation

This pipeline calculates T_{90} in the 50–300 keV energy range using the two NaI detectors. The main steps of automatic T_{90} calculation using the iteration method are as follows. First of all, our pipeline employs a quadratic polynomial function to fit the whole light curve, and then obtains the initial background fitting curve, as indicated by the magenta dot-dashed line in Figure 3. The data points, which are less than 3σ from the initial fitting curve, will be used as the updated background intervals.

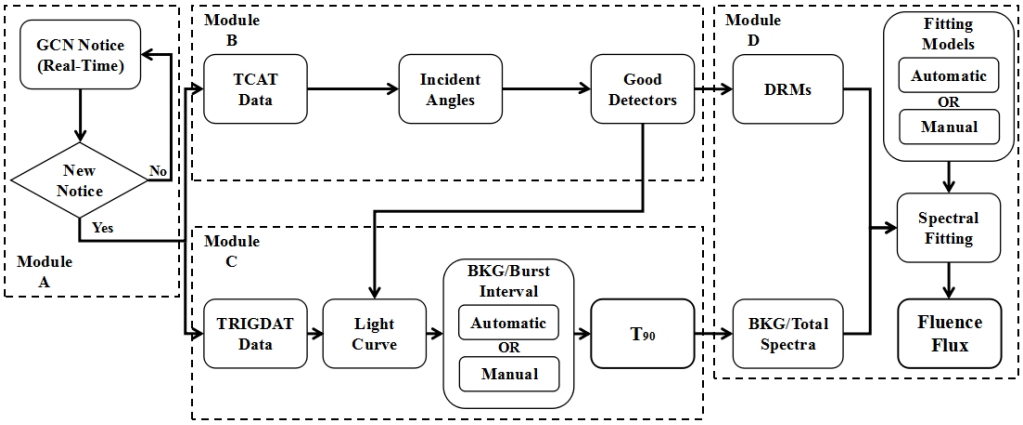

Fig. 2 The design of our low-latency light curve and spectral analysis pipeline.

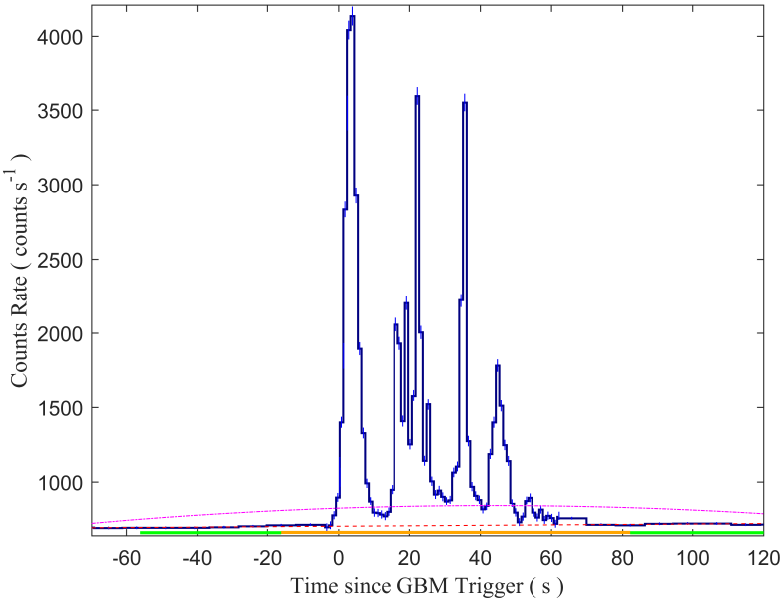

Fig. 3 Illustration of automatic T_{90} calculation, taking bn090626189 as an example. The *magenta dot-dashed line* is the initial background fitting curve and the *red dashed line* is the background fitting curve. The *orange horizontal line* is the burst interval used to calculate T_{90}, and the two *green horizontal lines* on both sides of the *orange horizontal line* are the final background intervals.

The pipeline uses a quadratic polynomial function to fit the updated background intervals, and then obtain the updated background fitting curve. After that, the pipeline will search for data points in the light curve which deviate from the updated background fitting curve by more than 4σ. Based on the time interval between these data points, our pipeline will define some time margin on both sides to include a part of the background as the burst interval, as shown by the orange horizontal line in Figure 3. Here we choose 18 s after a large value for testing the pipeline. The final background intervals are two 40 s intervals on both sides of the burst interval as shown by the two green horizontal lines in Figure 3. We found that the burst interval for most GRBs can be selected reasonably well by iterating once after a large number of tests (see Sect. 3.1). Thus we only iterate once for the sake of determining the final background intervals.

The background eventually adopted by our pipeline, as shown by the red dashed line in Figure 3, is given by a linear fitting to the final background intervals. The T_{90} is

calculated by accumulating the counts through the burst interval 5% to 95% above the background (Kouveliotou et al. 1993), which is different from T_{90} calculated by fluence accumulation in GBM (Goldstein et al. 2012). However, the comparison of T_{90} values suggests that these values calculated by the pipeline are basically consistent with those given by GBM (see Sect. 3.1). The error of T_{90} is computed by performing Monte-Carlo (MC) simulations considering statistical fluctuation of all data points during the burst interval. Only the Poisson error of data points caused by statistical fluctuation is considered.

Following this method, we analyzed bn090626189 as an example. Our automatically calculated T_{90} result for bn090626189 is consistent with the GBM result at the 1σ level, as listed in Table 1.

Table 1 The Calculation Result of bn090626189

	T_{90} (s)	T_{90} Start (s)	T_{90} End (s)
Our Automatic Result	46.46 ± 1.54	$T_0 + 1.41$	$T_0 + 47.87$
GBM Result	48.90 ± 2.83	$T_0 + 1.54$	$T_0 + 50.43$

We emphasize that the difference between manual and automatic calculations of T_{90} is obvious. The former selects the background and burst intervals manually, while the later automatically. The comparison of our automatically obtained T_{90} with those given by GBM will be discussed in Section 3.

2.4 Spectral Analysis

Using the background and T_{90} intervals calculated by the pipeline, the spectral analysis can be conducted. We performed the energy spectral fitting using *McSpecFit* (Zhang et al. 2016b), which is a software package that combines a Bayesian MC engine *McFit*, the general forward-folding algorithms and likelihood calculations. Particularly, the Bayesian MC engine (*McFit*) employs a Bayesian MC fitting algorithm to precisely fit the spectra (Zhang et al. 2016a). Previous researches show that the cutoff power law (CPL) model is preferred by most GRBs (e.g., Goldstein et al. 2012; Gruber et al. 2014; Yu et al. 2016), therefore we choose the CPL model in our pipeline to fit the spectra by default,

$$M_{\rm CPL}(E,P) = A\left(\frac{E}{E_{\rm piv}}\right)^{\alpha}\exp\left[-\frac{(\alpha+2)E}{E_{\rm peak}}\right], \quad (1)$$

where A is the amplitude, α is the low-energy spectral index, $E_{\rm peak}$ is the peak energy and $E_{\rm piv}$ is fixed to 100 keV. If the fitting fails, a power law model or a Band function (Band et al. 1993) will be used. The priors of all free parameters in the fitting are set to a uniform distribution, with the only exception being the amplitude which is set to a log distribution. With this algorithm, the best-fit spectral parameters and their uncertainties can be calculated by the converged MC chains. Thus the general forward-folding algorithms are used to compare a spectral model to data.

Then *McSpecFit* convolves the model with the DRMs to compare spectral models with the net count spectra,

$$C_M(I,P) = \int M(E,P)D(I,E)dE\,, \quad (2)$$

where $C_M(I,P)$ is the model-predicted count spectrum, $M(E,P)$ is the model spectrum and $D(I,E)$ represents the DRM. A forward-folding algorithm is used to deal with the GBM response $D(I,P)$ and read in the model spectra $M(E,P)$, then the count spectra will be fitted. $C_M(I,P)$ can be directly compared with the observed count spectra $C_O(I)$, as shown in Figure 4(a). Afterwards, *McSpecFit* calculates the likelihood for those $C_M(I,P)$ and $C_O(I)$ pairs. In the pipeline, the maximum likelihood-based statistics for Poisson data (Cash 1979) with Gaussian background (i.e. PGSTAT[5]) are used to estimate fitting parameters (see Figure 4(b)).

Finally the fluence is calculated from integration of the spectral model in 10–1000 keV. The error of the fluence is calculated with MC simulations.

Differently, the manual spectral analysis selects the background and burst intervals by the BA, and the fitting models can be recognized manually. The analyzed results of automatic and manual calculations of fluence will be discussed in Section 3.

3 PERFORMANCE OF THE PIPELINE

To examine the performance of this pipeline, we choose 700 *Fermi* GRBs before bn121211574 from the GBM catalog to test the reliability of the results. The TRIGDAT data of these GRBs meet the following conditions: (1) no less than three data points in the background intervals; (2) no less than one data point in the burst interval. The background and burst intervals are from the GBM catalog. In general, the pipeline takes $\sim$ 20 s to get T_{90}

[5] See also *https://heasarc.gsfc.nasa.gov/xanadu/xspec/manual/XSappendixStatistics.html.*

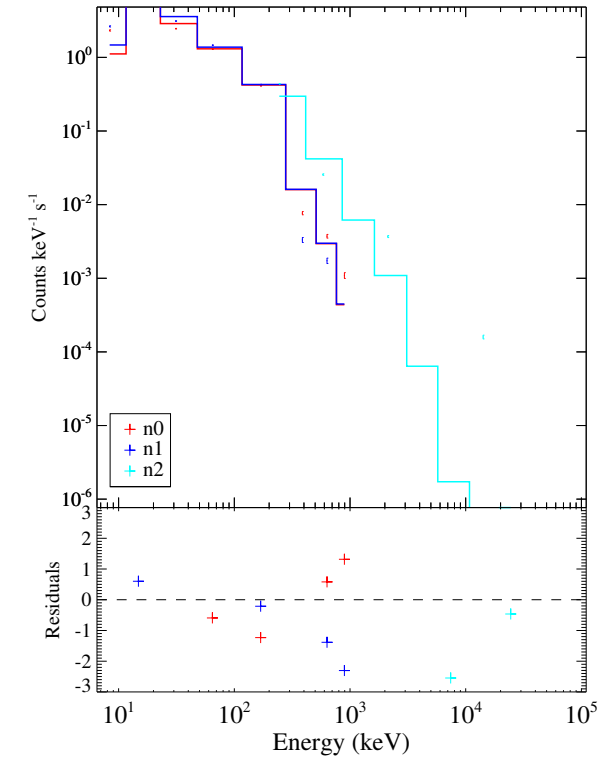

(a)

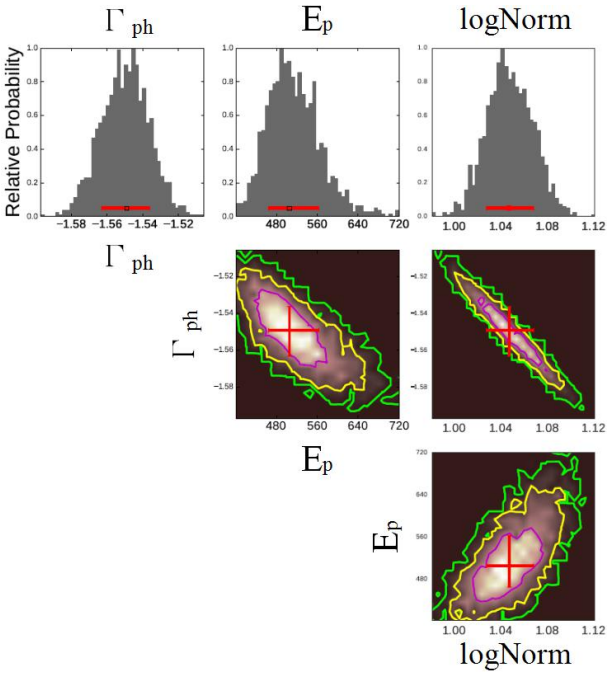

(b)

Fig. 4 Illustration of spectral fitting of bn090626189 with the CPL model. Panel (a): joint spectral fitting with the good detectors. Panel (b): the posterior corner maps given by *McSpecFit*. $\Gamma_{\rm ph}$, E_p and logNorm are the low-energy spectral index, the peak energy and the logarithmic amplitude of the CPL model, respectively.

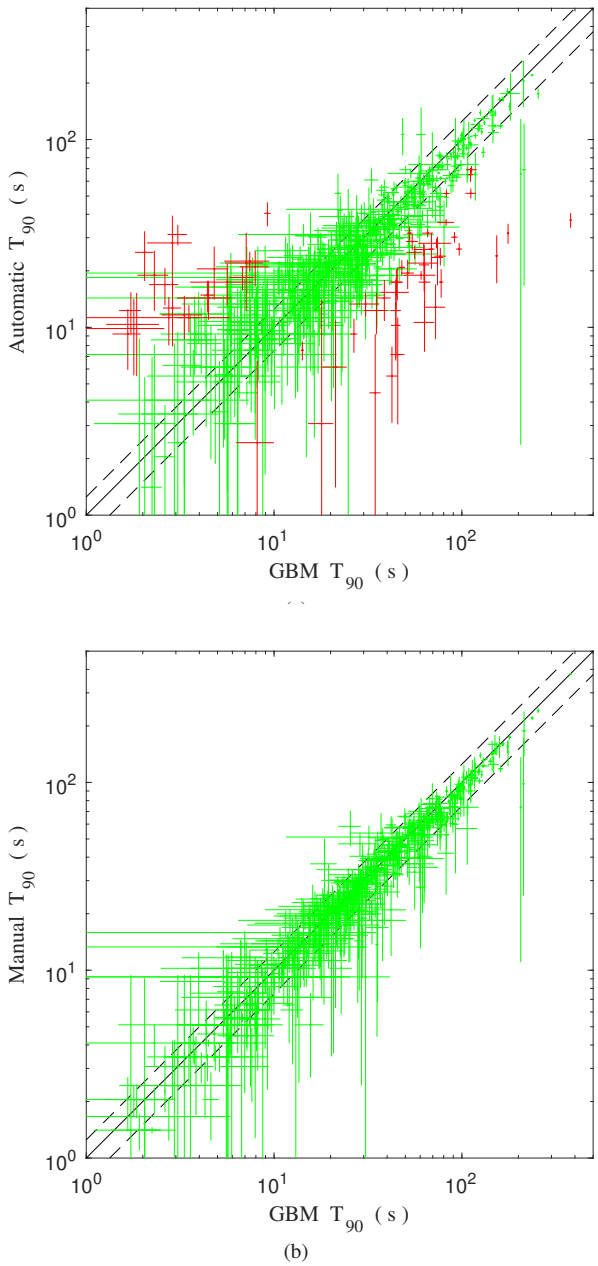

Fig. 5 Comparison between T_{90} obtained by our pipeline and those given by GBM. Panel (a): automatically calculated T_{90} versus those given by GBM. Panel (b): manually calculated T_{90} versus those given by GBM. *Green dots* are GRBs compatible with GBM results while *red dots* are GRBs incompatible with GBM results according to our criterion (see the text). *Diagonal solid lines* are $y = x$, and the *dashed lines* are $y = 0.75x$ and $y = 1.25x$.

and $\sim$ 5 min to obtain spectral fitting parameters and fluence. We compared our calculated results of T_{90} and fluence with the GBM catalog results (Goldstein et al. 2012; Gruber et al. 2014; Narayana Bhat et al. 2016).

The comparisons are shown in Figures 5 and 8. If our results are essentially in agreement with the GBM results, the data points should be distributed around the line $y = x$. We establish a criterion that the calculated results are considered acceptable if the data fall into the region between the line $y = 0.75x$ and $y = 1.25x$ within 2σ errors.

3.1 Comparison of T_{90}

According to this criterion, for $\sim 90\%$ of GRBs, our T_{90} values are consistent with those of GBM (see Fig. 5(a)).

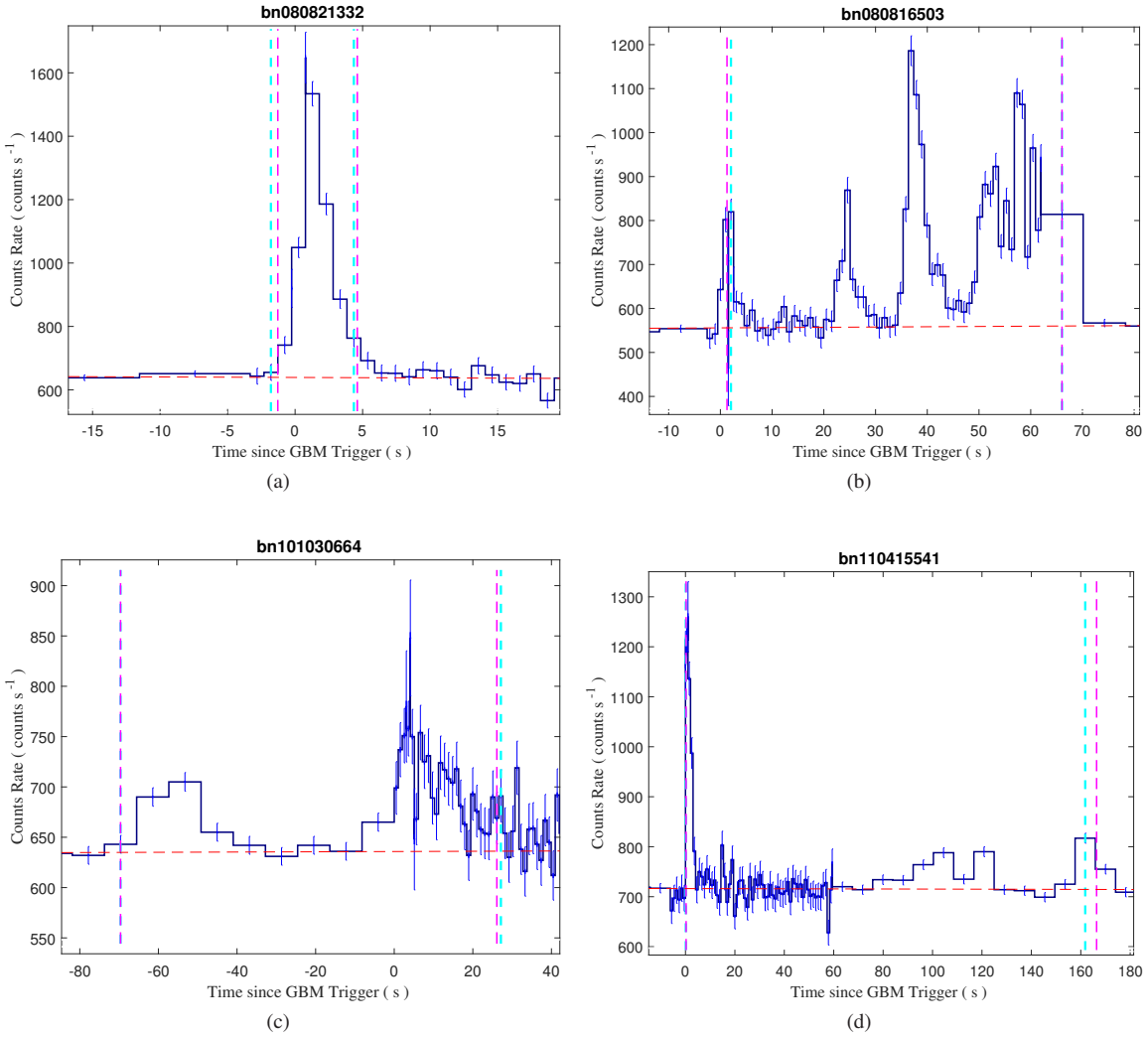

Fig. 6 The typical cases with reasonable T_{90} given by our automatic pipeline. The *red dashed lines* are the background fitting curves. The *light blue dashed lines* represent T_{90} obtained automatically, while the *magenta dashed lines* represent the T_{90} given by GBM.

After manually selecting the background and burst intervals, all GRBs are consistent with the GBM results, as displayed in Figure 5(b).

For most GRBs, our pipeline can give reasonable results as shown in Figure 6, demonstrating that our pipeline can provide very good results for typical GRB light curves. However, a small fraction of GRBs is not compatible with the GBM catalog results (see the red dots in Fig. 5). Figure 7 shows the inconsistent cases of calculated T_{90} given by our automatic pipeline.

For some inconsistent cases, such as bn100131730 and bn090817036, the results of T_{90} are shown in Figure 7(a) and (b), respectively. Judging from the light curves created by the TRIGDAT data, the emission of bn100131730 near $T_0 - 5$ s could be a part of the burst, which significantly exceeds the background; the count rate of bn090817036 near $T_0 - 10$ s and $T_0 + 30$ s cannot be distinguished from the background. It is worth noticing that the TRIGDAT data used to calculate T_{90} have coarse temporal and spectral resolution. The TTE data and the location of the bursts are required to accurately identify the burst intervals. However, to ensure its efficiency, our pipeline does not include this part of the analysis.

For other inconsistent cases, our pipeline fails to give the correct T_{90} in automatic runs (although manual processing can yield the right T_{90}). The main reason is that these GRBs present weak precursors or tails before or

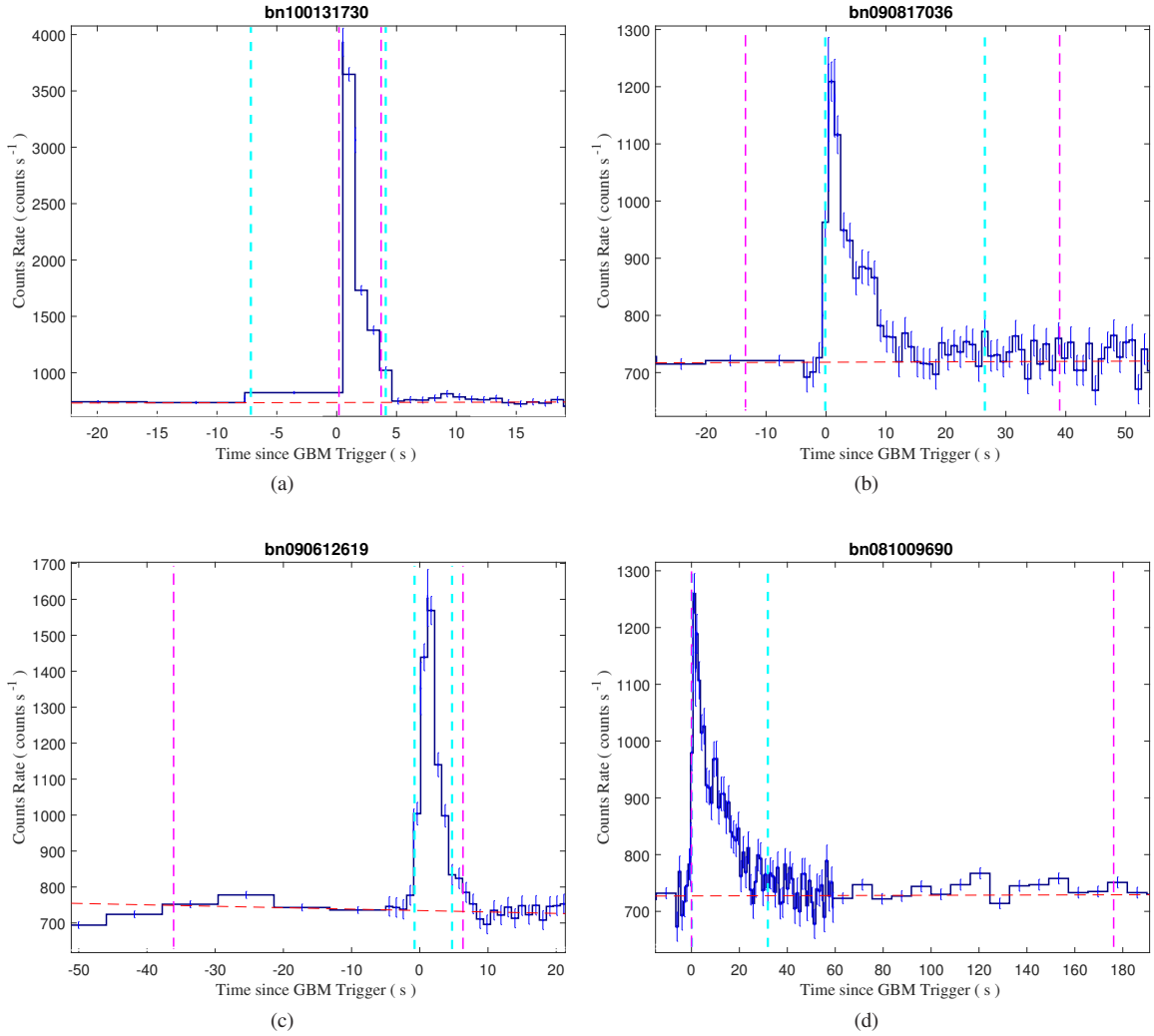

Fig. 7 The typical cases with badly calculated T_{90} given by our automatic pipeline. The definitions of *magenta lines* and *light blue lines* are the same as in Fig. 6.

after the main peaks. So far, our automatic T_{90} calculation cannot recognize precursors or tails with low significance, and sometimes even takes them as background intervals by mistake, which leads to much shorter T_{90} compared to the GBM results. Some examples can be seen in Figure 7(c) and (d).

Besides, for GRBs with T_{90} less than 1 s, neither manual nor automatic T_{90} calculations can give exact results due to the limited time resolution of the TRIGDAT data. However, our pipeline can automatically give the upper limit of T_{90} to determine whether a GRB is short or long, which plays an important role in the EM counterpart follow-ups. Actually, it is easy to identify the duration of a GRB manually in this case.

3.2 Comparison of Fluence

In order to compare the results of fluence with GBM, we used the same energy bands, time intervals and fitting model as those in the GBM catalog. As shown in Figure 8(a), for 92% of GRBs, the fluence is consistent with the GBM results when the pipeline runs automatically. This indicates that the majority of fluence can be calculated reasonably well by our pipeline.

It is worth mentioning that, for some GRBs, although the calculated T_{90} of our pipeline is not very consistent with the GBM catalog, there is no significant difference in the main emission components between our calculation and GBM results, as shown in Figure 7. Therefore, the fluence in these cases can also be calculated reliably, as tabulated in Table 2.

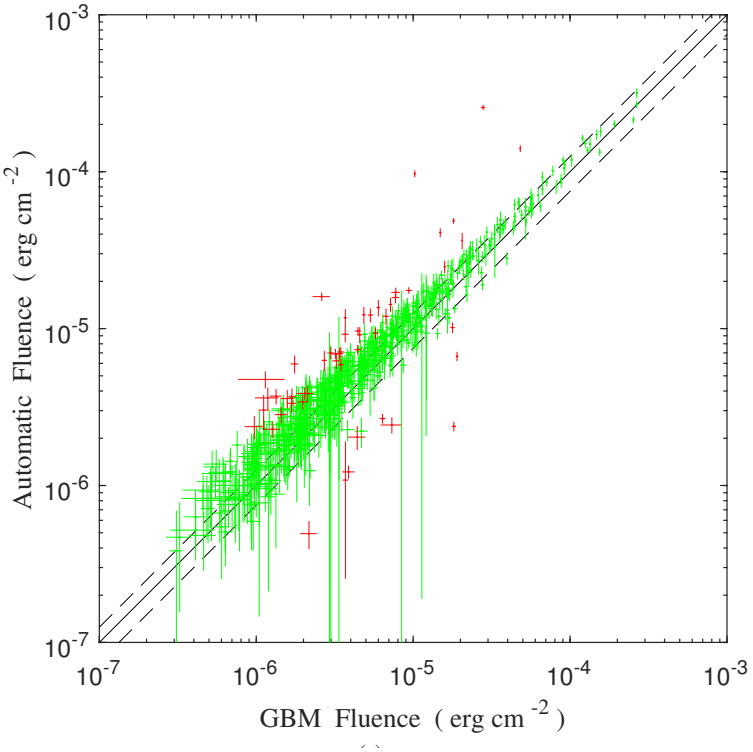

Fig. 8 Comparison between fluence obtained by this pipeline and those given by GBM. Panel (a): automatically calculated fluence versus those given by GBM. Panel (b): manually calculated fluence versus those given by GBM. The definitions of *green dots*, *red dots*, *solid lines* and *dashed lines* are the same as in Fig. 5.

Table 2 The Fluence Results of Four GRBs with Bad T_{90}

	bn100131730	bn090817036	bn090612619	bn081009690
Our Automatic T_{90} (s)	11.26 ± 1.95	26.62 ± 6.82	5.50 ± 2.24	31.74 ± 3.89
GBM T_{90} (s)	3.52 ± 0.45	52.42 ± 10.66	42.43 ± 2.89	176.19 ± 2.13
Fitting Models	CPL	CPL	CPL	CPL
Our Automatic Fluence ($\times 10^{-6}$ erg cm^{-2})	9.9 ± 2.0	4.2 ± 0.7	5.4 ± 2.0	12.8 ± 1.4
GBM Fluence ($\times 10^{-6}$ erg cm^{-2})	7.3 ± 0.2	5.6 ± 0.3	5.6 ± 0.3	9.0 ± 0.4

The main factors for the unreasonable automatically calculated fluence are: (1) the low energy resolution of the TRIGDAT data; (2) the unreasonably selected background and burst intervals by our automatic pipeline; (3) the DRMs affected by location accuracy and precision (Connaughton et al. 2015). After manually selecting the background intervals, the burst intervals and fitting models, the coincidence rate increases to 95%, as shown in Figure 8(b). However, the spectral resolution for the TRIRDAT data is fixed — only eight energy channels compared with 128 channels in the CSPEC and TTE data. The accuracy and precision of the GBM location recorded in the TCAT data also have a weak effect on the fluence through influencing the DRMs. Due to this intrinsic feature of the TRIGDAT data and some other problems such as the location-dependent DRMs, there are still $\sim 5\%$ of GRBs that are inconsistent with GBM catalog spectral results.

4 CONCLUSIONS AND DISCUSSION

In this paper, we developed an automatic low-latency pipeline for timing and spectral analysis based on *Fermi*/GBM near real-time data. Within $\sim$ 20 min after the GBM trigger, this pipeline can automatically accomplish timing and spectral analysis, and give some key parameters of GRBs, such as T_{90} and fluence. In addition to the ability to completely operate automatically, the pipeline allows for manually selecting background and burst intervals as well as spectral fitting models. For $\sim 90\%$ of GRBs, T_{90} and fluence are consistent with the GBM catalog results within 2σ errors when the pipeline runs automatically. While for manually selecting the background intervals, burst intervals and fitting models, the coincidence rate can increase to $\sim 95\%$ within 2σ errors.

The main goal of this pipeline is to support the follow-up observation strategy of POLAR by providing the earliest T_{90} and fluence after the GBM trigger. Low latency calculation of these properties could play an important role in joint and follow-up observations. If a GRB satisfies some criteria (e.g. long GRB with large fluence or short GRB), alerts for follow-up observations could be sent out at the earliest time. Moreover, the pipeline is also serving for the *Insight* Hard X-Ray Modulation Telescope (*Insight*-HXMT), the first Chinese X-ray space telescope which is able to detect GRBs and EM counterparts of GW events (Li et al. 2018). This pipeline has been used by POLAR and *Insight*-HXMT, and will be open to the astronomical community.

The detection and research of GWs and their prompt EM counterparts have increased significantly of late. Previous studies suggest that short-duration GRBs are likely to be generated by the mergers of binary neutron stars (BNSs) or a neutron star and a black hole (Fernández & Metzger 2016). Thus they are usually considered to be the high-energy EM counterparts of GWs. Recently, LIGO/Virgo, *Fermi*/GBM and INTEGRAL/SPI-ACS have jointly found the first GW event GW170817 together with its prompt EM counterpart GRB 170817A (Abbott et al. 2017a,b,c) originating from the first known BNS merger.

After receiving the GBM trigger notice, this pipeline immediately processed the near real-time data of GRB 170817A, and provided preliminary information 21 min after the GBM trigger. It reported that the fluence of GRB 170817A is $(3.3 \pm 0.7) \times 10^{-7}$ erg cm^{-2}, which is consistent with $(2.8 \pm 0.2) \times 10^{-7}$ erg cm^{-2} (Goldstein et al. 2017) at the 1σ level.

It is anticipated that more GW events generated by mergers of BNSs and their EM counterparts will be found in the near future. With our pipeline, primary timing and spectral information about GRBs can be calculated and reported rapidly, which is of great importance for follow-up EM counterpart observations.

The main advantages of this pipeline are low-latency and automatic operation. For most GRBs, our pipeline can give quite reliable results, though it does not work well for a small fraction of bursts with very special light

curves. We emphasize, however, this may be partially, if not totally, due to the intrinsic low temporal and spectral resolution of the near real-time data (TRIGDAT, TCAT) that the pipeline used.

Continuous improvements in this pipeline are ongoing. The first step is to estimate the in-flight background of GBM using a direction dependent background fitting (DDBF) method (Szécsi et al. 2013) or to estimate the background level from the last 30 or 60 orbits (Fitzpatrick et al. 2011). The second step is to introduce the deep learning method (Lecun et al. 2015) to intelligently distinguish background and burst intervals and to select suitable fitting models. With these improvements, the background and burst intervals of GRBs could be distinguished better by the pipeline and more reliable results for temporal and spectral analysis can be obtained.

Acknowledgements We thank the anonymous reviewer for helpful comments and suggestions. This work is supported by the Strategic Priority Research Program of the Chinese Academy of Sciences (Grant No. XDB23040400), the National Natural Science Foundation of China (Grant Nos. 11403026, 11503028 and 11673023) and the National Basic Research Program of China (973 program, Grant No. 2014CB845800). BBZ acknowledges support from the National Thousand Young Talents program of China. We gratefully acknowledge support from the collaboration team of POLAR, a project funded by China National Space Administration (CNSA), the Chinese Academy of Sciences (CAS) and the University of Geneva (UNIGE). The authors would also like to thank Jing Jin, Jinlu Qu, Xiaobo Li, Youli Tuo, Zijian Li, Mingyu Ge, Jinyuan Liao, Guangcheng Xiao, Yue Huang and Chengkui Li for their suggestions on data analysis and the revision of this paper.

References

Abbott, B. P., Abbott, R., Abbott, T. D., et al. 2017a, ApJ, 848, L12
Abbott, B. P., Abbott, R., Abbott, T. D., et al. 2017b, ApJ, 848, L13
Abbott, B. P., Abbott, R., Abbott, T. D., et al. 2017c, Physical Review Letters, 119, 161101
Band, D., Matteson, J., Ford, L., et al. 1993, ApJ, 413, 281
Berger, E. 2014, ARA&A, 52, 43
Boella, G., Butler, R. C., Perola, G. C., et al. 1997, A&AS, 122, 299
Cash, W. 1979, ApJ, 228, 939
Connaughton, V., Briggs, M. S., Goldstein, A., et al. 2015, ApJS, 216, 32
Fernández, R., & Metzger, B. D. 2016, Annual Review of Nuclear and Particle Science, 66, 23
Fitzpatrick, G., Connaughton, V., McBreen, S., & Tierney, D. 2011, arXiv:1111.3779
Gehrels, N., Chincarini, G., Giommi, P., et al. 2004, ApJ, 611, 1005
Goldstein, A., Burgess, J. M., Preece, R. D., et al. 2012, ApJS, 199, 19
Goldstein, A., Veres, P., Burns, E., et al. 2017, ApJ, 848, L14
Gruber, D., Goldstein, A., Weller von Ahlefeld, V., et al. 2014, ApJS, 211, 12
Klebesadel, R. W., Strong, I. B., & Olson, R. A. 1973, ApJ, 182, L85
Kole, M., Li, Z. H., Produit, N., et al. 2017, Nuclear Instruments and Methods in Physics Research A, 872, 28
Kouveliotou, C., Meegan, C. A., Fishman, G. J., et al. 1993, ApJ, 413, L101
Kumar, P., & Zhang, B. 2015, Phys. Rep., 561, 1
Lazzati, D. 2006, New Journal of Physics, 8, 131
Lecun, Y., Bengio, Y., & Hinton, G. 2015, Nature, 521, 436
Li, T., Xiong, S., Zhang, S., et al. 2018, Science China Physics, Mechanics, and Astronomy, 61, #31011
Lin, Y.-Q. 2009, RAA (Research in Astronomy and Astrophysics), 9, 682
Meegan, C., Lichti, G., Bhat, P. N., et al. 2009, ApJ, 702, 791
Narayana Bhat, P., Meegan, C. A., von Kienlin, A., et al. 2016, ApJS, 223, 28
Orsi, S., Haas, D., Hajdas, W., et al. 2011, Nuclear Instruments and Methods in Physics Research A, 648, 139
Paciesas, W. S., Meegan, C. A., von Kienlin, A., et al. 2012, ApJS, 199, 18
Produit, N., Barao, F., Deluit, S., et al. 2005, Nuclear Instruments and Methods in Physics Research A, 550, 616
Produit, N., Bao, T. W., Batsch, T., et al. 2018, Nuclear Instruments and Methods in Physics Research A, 877, 259
Suarez-Garcia, E., Haas, D., Hajdas, W., et al. 2010, Nuclear Instruments and Methods in Physics Research A, 624, 624
Szécsi, D., Bagoly, Z., Kóbori, J., Horváth, I., & Balázs, L. G. 2013, A&A, 557, A8
Toma, K., Sakamoto, T., Zhang, B., et al. 2009, ApJ, 698, 1042
von Kienlin, A., Meegan, C. A., Paciesas, W. S., et al. 2014, ApJS, 211, 13
Xiong, S., Produit, N., & Wu, B. 2009, Nuclear Instruments and Methods in Physics Research A, 606, 552
Yu, H.-F., Preece, R. D., Greiner, J., et al. 2016, A&A, 588, A135
Zhang, B. 2011, Comptes Rendus Physique, 12, 206
Zhang, B.-B., Uhm, Z. L., Connaughton, V., Briggs, M. S., & Zhang, B. 2016a, ApJ, 816, 72
Zhang, B.-B., Zhang, B., Castro-Tirado, A. J., et al. 2016b, arXiv:1612.03089